International Journal of Nanomedicine

Dovepress
open access to scientific and medical research

Open Access Full Text Article

ORIGINAL RESEARCH

Inhibition of heat-shock protein 90 sensitizes liver cancer stem-like cells to magnetic hyperthermia and enhances anti-tumor effect on hepatocellular carcinoma-burdened nude mice

This article was published in the following Dove Press journal:
International Journal of Nanomedicine
7 December 2015
Number of times this article has been viewed

Rui Yang[1,*]
Qiusha Tang[1,*]
Fengqin Miao[1]
Yanli An[2]
Mengfei Li[1]
Yong Han[1]
Xihui Wang[1]
Juan Wang[3]
Peidang Liu[1]
Rong Chen[4]

[1]School of Medicine, Southeast University, [2]Jiangsu Key Laboratory of Molecular and Functional Imaging, Department of Radiology, Zhongda Hospital, Nanjing, [3]Department of Infectious Disease, The Third People's Hospital of Nantong, Nangtong; [4]Department of Oncology, Zhongda Hospital, Nangjing, Jiangsu Province, People's Republic of China

*These authors contributed equally to this work

Purpose: To explore the thermoresistance and expression of heat-shock protein 90 (HSP90) in magnetic hyperthermia-treated human liver cancer stem-like cells (LCSCs) and the effects of a heat-shock protein HSP90 inhibitor 17-allylamino-17-demethoxgeldanamycin (17-AAG) on hepatocellular carcinoma-burdened nude mice.

Methods: $CD90^+$ LCSCs were isolated by magnetic-activated cell sorting from BEL-7404. Spheroid formation, proliferation, differentiation, drug resistance, and tumor formation assays were performed to identify stem cell characteristics. CD90-targeted thermosensitive magnetoliposomes (TMs)-encapsulated 17-AAG (CD90@17-AAG/TMs) was prepared by reverse-phase evaporation and its characteristics were studied. Heat tolerance in $CD90^+$ LCSCs and the effect of CD90@17-AAG/TMs-mediated heat sensitivity were examined in vitro and in vivo.

Results: $CD90^+$ LCSCs showed significant stem cell-like properties. The 17-AAG/TMs were successfully prepared and were spherical in shape with an average size of 128.9±7.7 nm. When exposed to magnetic hyperthermia, HSP90 was up-regulated in $CD90^+$ LCSCs. CD90@17-AAG/TMs inhibited the activity of HSP90 and increased the sensitivity of $CD90^+$ LCSCs to magnetic hyperthermia.

Conclusion: The inhibition of HSP90 could sensitize $CD90^+$ LCSCs to magnetic hyperthermia and enhance its anti-tumor effects in vitro and in vivo.

Keywords: thermoresistance, $CD90^+$ LCSCs, magnetic hyperthermia, 17-AAG

Introduction

Recently, magnetic hyperthermia has been widely used for the treatment of hepatic carcinoma, bladder cancer, and breast cancer in vitro and in vivo.[1–3] However, the emergence of thermoresistance in tumor cells upon subsequent heating could prevent apoptosis and result in fewer dead cells.[4,5] Heat-shock proteins (HSPs) are associated with thermoresistance and the induction of the heat-shock response, in particular, the up-regulation of HSP90, can impact upon the effect and duration of thermoresistance. Inhibiting HSP90 can sensitize tumor cells to hyperthermia and can result in increased tumor cell apoptosis.[6] In a previous study, a nano-particle-conjugated HSP90 inhibitor was able to promote tumor cell apoptosis under low-temperature magnetic hyperthermia conditions.[7] It has been reported that using 17-AAG could overcome the thermoresistance and enhance the apoptosis of cancer cell induced by gold nanoparticle-mediated hyperthermia.[8] 17-AAG is an HSP90 inhibitor derived from the geldanamycin antibiotic and can kill tumor cells by reversibly associating with HSP90. It has often been given by intravenous injection in an organic solvent due to its poor solubility in water

Correspondence: Qiusha Tang
School of Medicine, Southeast University, 87 Dingjiaqiao Road, Nanjing 210009, Jiangsu Province, People's Republic of China
Tel +86 25 8327 2373
Fax +86 25 8327 2541
Email panyixi-tqs@163.com

and low oral bioavailability, which can cause serious side effects.[9] Therefore, a new method of treatment is needed for this compound to replace the toxic organic solvent.

Liver cancer stem-like cells (LCSCs) are a chemoresistant subpopulation that is capable of self-renewal and tumor initiation. An increasing number of studies have shown that CD90, which is expressed by hepatic stem/progenitor cells during liver development, could be used as a marker for human LCSCs and as a target for the diagnosis and therapy of hepatocellular carcinoma (HCC).[10–12] Therefore, $CD90^+$ LCSCs are referred to as $CD90^+$ LCSCs in this study. Relapse and metastases can occur if the applied treatments fail to remove cancer stem cells (CSCs); therefore, therapies that eliminate CSCs may be more effective than current drugs that target proliferating non-CSCs in the treatment of HCC. Studies have shown that CSCs could be effectively eliminated by magnetic hyperthermia in some cases. Moreover, magnetic hyperthermia can significantly delay tumor initiation and formation.[13] Hence, magnetic hyperthermia may be a novel therapy for treating chemotherapy and radiotherapy-tolerant CSCs.

In the previous study, CD90-targeted TMs for 17-AAG were synthesized that contained no organic solvent. The TM nanocarrier system was manipulated to release 17-AAG when the temperature reached the phase transition temperature (T_m), which occurs when the TMs are localized in an alternating current magnetic field (ACMF) in the cells. This previous study also demonstrated for the first time that CD90@17-AAG/TMs could effectively kill $CD90^+$ LCSCs in vitro and in vivo by inhibiting HSP and enhancing hyperthermia responsiveness.

Materials and methods

Cells and animals

BEL-7404 cells were purchased from the Institute of Biochemistry and Cell Biology (Shanghai Institute of Biological Sciences, Chinese Academy of Sciences). Cells were cultured in Dulbecco's Modified Eagle's Medium (DMEM) medium (Thermo Fisher Scientific, Waltham, MA, USA) supplemented with 10% fetal bovine serum (FBS, Thermo Fisher Scientific), 100 U/mL penicillin, and 100 mg/mL streptomycin, and were maintained at 37°C in 5% CO_2 in a humidified incubator. $CD90^+$ LCSCs were isolated from BEL-7404 cell lines by magnetic-activated cell sorting (MACS), and cultured with DMEM/F12 (1:1) (Thermo Fisher Scientific) containing 20 μg/L recombinant human epidermal growth factor, 20 μg/L basic fibroblast growth factor, and 2% B27 in a low-adhesion culture bottle.

BALB/C nude mice (female, aged 5 weeks) were purchased from the Comparative Medicine Centre of Yangzhou University (Jiangsu, People's Republic of China). The human cell line and animal studies were approved by the ethics committee of Southeast University, Nanjing, People's Republic of China. Patient consent was not required for using human cell lines. All animals received humane care in compliance with the Principles of Laboratory Animal Care formulated by the National Society for Medical Research.

Chemicals

A MidiMACS starting kit was purchased from Miltenyi Biotec (Bergisch Gladbach, Germany). Dipalmitoylphosphatidylcholine (DPPC) and 1,2-distearoyl-sn-glycero-3-phosphoethanolamine-*N*-[methoxy (polyethylene glycol)-2000] (PEG_{2000}-DSPE) were purchased from Corden Pharma (Cambridge, MA, USA). Maleicamide-PEG_{2000}-DSPE (Mal-PEG_{2000}-DSPE) was purchased from Laysan Bio (Arab, AL, USA) and 17-AAG was purchased from LC Laboratories (Woburn, MA, USA). All solvents were of high-performance liquid chromatography grade.

Synthesis of CD90-modified 17-AAG incorporated TMs

Fe_3O_4 was prepared as described by Li et al using chemical co-precipitation.[14] 17-AAG/TMs were prepared by the thin-film hydration method.[15] Briefly, DPPC, cholesterol, $mPEG_{2000}$-DSPE, and 17-AAG (molar ratio, 54:6:1:1) in methanol and chloroform (v/v, 3:2) were evaporated at 42°C to form a dry lipid film. Then, the film was hydrated with phosphate-buffered saline (PBS, pH =7.4) and mixed with Fe_3O_4 (2 mg/mL) at 60°C for 1 hour to get 17-AAG/TMs. 17-AAG-loaded thermosensitive liposomes (17-AAG/TSLs) and TMs were prepared through a similar method. Anti-CD90 modifying was performed as previously described.[16]

Characterization of CD90@17-AAG/TMs

Morphology, diameter, and size distribution analysis

The ultrastructural morphology of CD90@17-AAG/TMs was observed through transmission electron microscopy (Hitachi, Tokyo, Japan). Liposome size in water was determined using ZetaPlus analysis (Brookhaven Instruments Co., Holtsville, NY, USA).

Quantification of 17-AAG and Fe_3O_4 by UV–Vis spectrophotometry

The amount of 17-AAG incorporated in TMs was quantified by ultraviolet–visible (UV–Vis) spectrophotometry at a detection wavelength of 333 nm. Iron content was measured using 1,10-phenanthroline spectrophotometry as described by Wu et al.[17]

T_m and drug release of 17AAG-TMs

T_m of 17-AAG/TMs was observed by differential scanning calorimetry. The release of 17-AAG from 17-AAG/TMs in vitro was evaluated in PBS (pH 7.4) at 25°C, 37°C, 43°C, 55°C, and 65°C by the dynamic dialysis method as performed previously. The UV–Vis absorption spectra of released 17-AAG within 72 hours were detected at different temperatures. The 17-AAG content in the dialysate was quantified.

Increasing temperature tests and specific absorption rate

The increasing temperature test was performed as described previously.[18] Briefly, CD90@17-AAG/TMs and 17-AAG/TMs were diluted by PBS (pH 7.4) to retain the same Fe concentrations. The blank TSLs were used as control. Then, the solution was placed on an ACMF generated by an SPG-06A high-frequency induction heater from Shenzhen, People's Republic of China (f=200 kHz; I=20 A) for 60 minutes. The temperature was observed every 5 minutes. The specific absorption rate value was calculated as described by Xie et al.[19]

Storage stability of CD90@17-AAG/TMs

Measurement of storage stability was performed at 4°C for 4 weeks. The particle size and drug encapsulation efficiency were detected at 0 hour, 8 hours, 16 hours, 24 hours, 1 day, 7 days, 14 days, and 21 days.

Cell sorting and culture

$CD90^+$ LCSCs were sorted from BEL-7404 cells according to the manufacturer's instructions (Miltenyi Biotec). BEL-7404 cells were labeled with CD90 MicroBeads at 4°C for 30 minutes in the buffer we prepared (PBS containing 2% bovine serum albumin and 10 mM ethylenediaminetetraacetic acid). The cells were sorted on a MiniMACS column after being washed three times. The $CD90^+$ LCSCs were plated at a density of 10^5 cell/mL in DMEM/F12 media in a low-adhesion culture plate to form spheroids of LCSCs.

Identification of stem cell characteristics

Proliferation assay

The assay was performed to evaluate the proliferative ability of the $CD90^+$ LCSCs and $CD90^-$ BEL-7404 cells sorted from BEL-7404 cells. The same number of cells was planted on a 96-well plate. CCK-8 reagent was added to the plate at 1, 3, 5, and 7 days and the absorbance was measured at 450 nm.

Differentiation assay

$CD90^+$ LCSCs were cultured with DMEM medium supplemented with 10% FBS. At 1, 3, 5, and 7 days, cells were collected and incubated with FITC-conjugated anti-CD90 monoclonal antibody at 4°C for 30 minutes, and then analyzed by a flow cytometry (FCM, BD Biosciences, San Jose, CA, USA).

Drug resistance assay

$CD90^+$ LCSCs and $CD90^-$ BEL-7404 cells were cultured with different concentrations of doxorubicin (DOX), 5-fluorouracil (5-FU), and oxaliplatin (OXA) at 37°C for 24 hours. The number of cells in each sample was quantified using a CCK-8 assay by measuring absorbance at 450 nm. The rate of cell growth inhibition was calculated by the formula: Inhibition rate = (OD value of the control group − OD value of experimental group)/(OD value of the control group − OD value of blank Group). Drug doses to inhibit 50% of cell growth (IC50 values) were then calculated by a modified Kou-type method: lg IC50 = Xm-I (P-(3-Pm-Pn)/4), where Xm: lg Maximum dose; I: lg (maximum dose/adjacent dose); P: sum of positive response rate; Pm: the largest positive response rate; Pn: the smallest positive response rate.

In vivo tumorigenicity assay

$CD90^+$ and $CD90^-$ cells sorted from BEL-7404 cells were resuspended in 150 μL of PBS, and then injected (1×10^5 cells/injection) into the right forelimb of BALB/C nude mice. The mice were examined every 2 days. Hematoxylin and eosin (H&E) staining and immunohistochemical (IHC) staining were used to detect the expression of CD90.

Effects of magnetic hyperthermia on apoptosis rate and the expression of HSP90 and caspase-3

$CD90^+$ LCSCs were incubated with the TMs coupled with anti-CD90 (CD90@TMs) (hyperthermia temperature, 43°C, called TMs group) for 24 hours and then were placed on an ACMF (f=200 kHz; I=20 A) to heat for 1 hour. Control group (cells incubated with DMEM) was not heated. Apoptosis rates were measured by FCM using an apoptosis detection kit (Beyotime Institute of Biotechnology, Shanghai, People's Republic of China) according to the manufacturer's instructions. The expression of HSP90 was determined by Western blotting after 10 minutes, 4 hours, 8 hours, 12 hours, and 24 hours of culture time after heat treatment. To determine if the inhibition of HSP90 could sensitize $CD90^+$ LCSCs to magnetic hyperthermia, the expression of caspase-3 was examined by Western

blotting 24 hours after heat treatment. To investigate the effect of HSP90 on the susceptibility of CD90$^+$ LCSCs to hyperthermia susceptibility, 17-AAG was incubated with the cells before they were heated (called 17-AAG/TMs). The rate of apoptosis rates and the expression of HSP90 were then detected.

Inhibition CD90$^+$ LCSCs in vitro using CD90@17-AAG/TMs

To determine if inhibiting HSP90 could sensitize CD90$^+$ LCSCs to magnetic hyperthermia, cells were divided into ten groups to receive the following treatments: 1) control group (cells incubated with DMEM); 2) TM treatment group (cells incubated with TMs and unexposed to ACMF); 3) TMs + ACMF group (cells incubated with TMs and exposed to ACMF); 4) 17-AAG/TSLs group (cells incubated with 17-AAG/TSLs/TSLs); 5) 17-AAG/TMs + ACMF group (cells incubated with 17-AAG/TMs and exposed to ACMF); 6) CD90@TMs + ACMF group (cells incubated with 17-AAG/TMs and exposed to ACMF); 7) TSLs group (cells incubated with TSLs); 8) 17-AAG group (cells incubated with 17-AAG); and 9) ACMF group (cells incubated with DMEM and exposed to ACMF); and 10) 17-AAG/TMs + ACMF group (cells incubated with 17-AAG/TMs and exposed to ACMF). The apoptosis rate of cells in each group was observed by FCM.

Inhibition of tumor growth in CD90$^+$ LCSCs-bearing mice by HSP90 inhibition and magnetic hyperthermia

CD90$^+$ LCSCs (5×10^6 cells) were implanted in the right legs of BALB/C mice. When the tumor volume reached approximately 600 mm^3, the mice were randomly divided into nine groups: control group; TMs + ACMF group (tumors injected with TMs and exposed to ACMF); 17-AAG/TSLs group (tumors injected with 17-AAG/TSLs); 17-AAG/TMs + ACMF group (tumors injected with 17-AAG/TMs and exposed to ACMF); CD90@TMs + ACMF group (tumors injected with CD90@TMs and exposed to ACMF); TSLs group (tumors injected with TSLs); 17-AAG group (tumors injected with 17-AAG); ACMF group (tumors injected with DMEM and exposed to ACMF) and CD90@17-AAG/TMs + ACMF group (tumors injected with CD90@17-AAG/TMs and exposed to ACMF). Each group contained six mice. The nanoparticles were directly injected into the tumors as previously described.[17] After 24 hours, the hyperthermia groups were placed on an ACMF (f=200 kHz; I=20 A) for 60 minutes every other day. The maximal temperature of the rectal tissue did not exceed 40°C. Tumor volume was calculated as follows: (long diameter × short diameter^2)/2. Seven days later, the mice were euthanized, and then sectioned with H&E staining. The cell apoptosis rate in vivo was determined by a transferase-mediated deoxyuridine triphosphate-biotin nick end labeling (TUNEL) assay according to the manufacturer's instructions (Roche, Pleasanton, CA, USA). To assess the fraction of apoptotic cells, the count of TUNEL-positive cells was calculated from five sections.

Statistical analysis

Values are presented as means ± standard deviation (SD). The data were analyzed using SPSS for Windows software (ver. 16.0; SPSS Inc., Chicago, IL, USA). A P-value of <0.05 was considered significant.

Results and discussion

Characterization of CD90@17-AAG/TMs

CD90@17-AAG/TMs were synthesized following thin-film hydration method methodology. The surface morphology of CD90@17-AAG/TMs was evaluated by transmission electron microscopy. As shown in Figure 1A, the average vesicle diameter was approximately 90–100 nm. The diameter of 17-AAG/TMs in water was 128.9±7.7 nm (Figure 1B). TSLs are well-studied nanocarriers for drugs that can release drugs in a controlled manner at the target site by altering temperature. The encapsulation rate of 17-AAG was 93.8%, and the Fe content was 3.5 mg/mL. The T_m of CD90@17-AAG/TMs was examined by differential scanning calorimetry, and there was little difference in T_m between CD90@17-AAG/TMs and pure DPPC (41.9°C vs 42°C). The release of 17-AAG from the CD90@17-AAG/TMs at pre-set temperatures was determined by UV–Vis spectrometry at 331 nm (Figure 1C). The cumulative release curve (Figure 1D) showed a controlled release of 17-AAG from the lipid bilayer in PBS at 37°C and 43°C. Only 39.85% of 17-AAG from CD90@17-AAG/TMs was released within 72 hours at 37°C. When the temperature averaged 43°C, drug release increased significantly (approximately 54.28% within 72 hours). A fast release of 17-AAG occurred within the first 2 hours, and there was an initial release burst from the liposomal formulation at 55°C and 65°C. At this time point, nearly 50% of 17-AAG at 55°C and 78.69% of 17-AAG at 65°C leaked from the liposomes. In addition, approximately 97.1% of 17-AAG had permeated the dialysis tubing by 24 hours at 65°C. Conversely, 17-AAG showed almost no release at 25°C. In conclusion, CD90@17-AAG/TMs showed good thermal response, and when the formulations were injected in vivo, the TMs should release the 17-AAG in

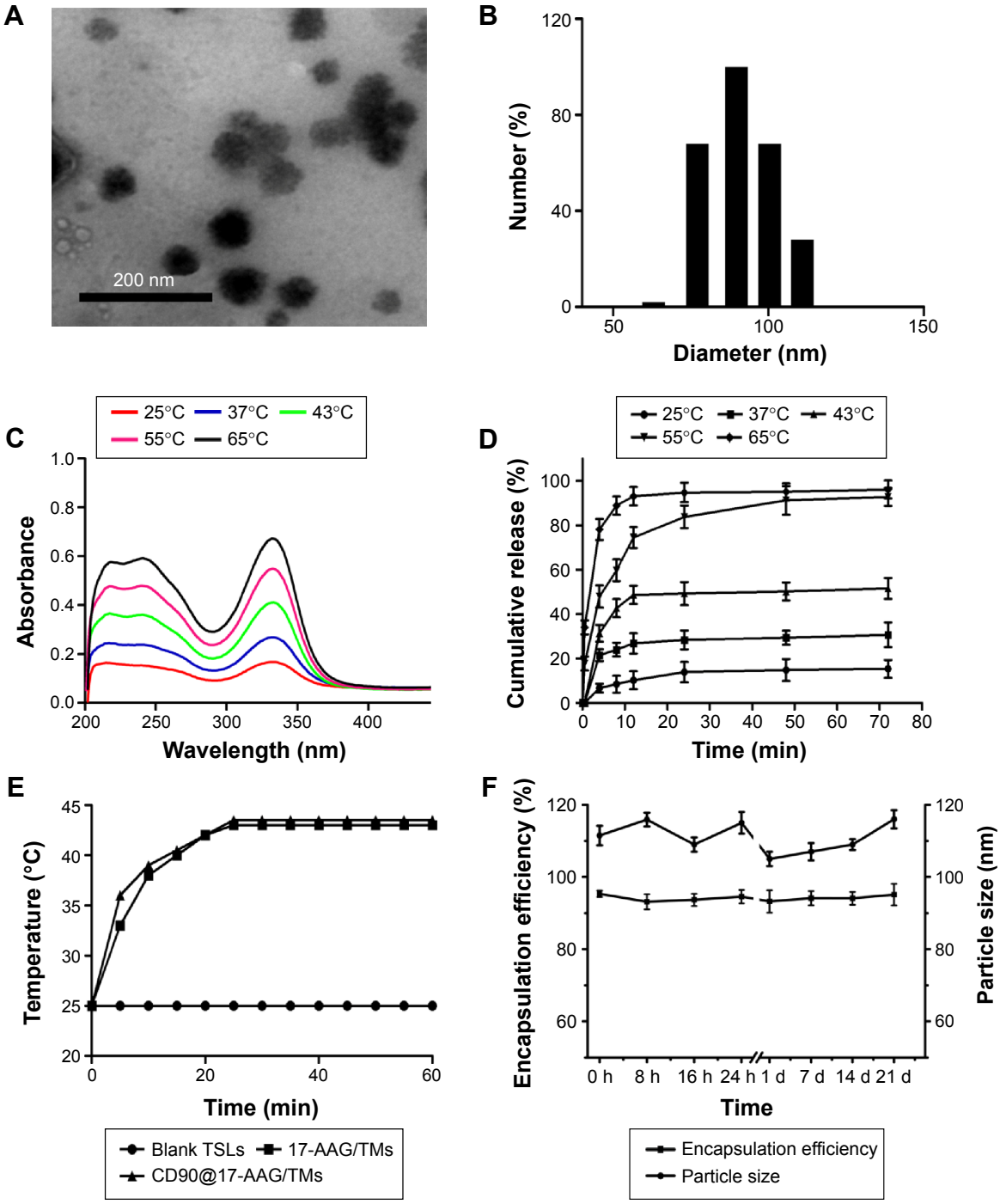

Figure 1 Characterization of CD90@17-AAG/TMs.

Notes: (**A**) Surface morphology of CD90@17-AAG/TMs in TEM. **(B)** Size distribution and size in water of CD90@17-AAG/TMs. **(C)** UV/Vis absorption spectra of released 17-AAG at different temperatures at 72h. **(D)** Cumulative release curve of 17-AAG from CD90@17-AAG/TMs. **(E)** Heating curve of CD90@17-AAG/TMs and 17-AAG/TMs in an ACMF for 60 min using an electric current of 20 A and a frequency of 200 kHz. **(F)** Storage stability of CD90@17-AAG/TMs in PBS (pH 7.4) at 4°C.

Abbreviations: CD90@17-AAG/TMs, CD90-targeted thermosensitive magnetoliposomes-encapsulated 17-AAG; d, day/s; h, hours; min, minutes; TMs, thermosensitive magnetoliposomes; TEM, transmission electron microscope; UV, ultraviolet; Vis, visible; ACMF, alternating current magnetic field; PBS, phosphate-buffered saline; TSLs, thermosensitive liposomes; 17-AAG, 17-allylamino-17-demethoxgeldanamycin; 17-AAG/TMs, thermosensitive magnetoliposomes-encapsulated 17-AAG.

the tumor when exposed to ACMF, but not in normal tissues. There was little difference in heating capacity between CD90@17-AAG/TMs and 17-AAG/TMs when placed in an ACMF (Figure 1E), and the heating curves were well controlled when the temperature was increased. Meanwhile, blank TSLs did not change with temperature. CD90@17-AAG/TMs had a specific absorption rate value of 74.1 w/g, which was determined by an electric current of 20 A and a frequency of 200 kHz. The storage stability of CD90@17-AAG/TMs in PBS (pH 7.4) at 4°C is shown in Figure 1F. The

particle size and drug entrapment efficiency barely changed over 4 weeks, which suggests good storage ability.

Identification of stem cell characteristics

In an attempt to identify the stem cell-like properties of $CD90^+$ BEL-7404 cells, spheroid colony formation assay were first performed in vitro in a low-adhesion culture plate with serum-free DMEM/F12 media containing only growth factors. As shown in Figure 2A, $CD90^+$ BEL-7404 cells produced colonies after 7 days, which demonstrated their capacity for self-renewal.

To further examine stem cell properties, proliferation and differentiation capacity were assessed by a CCK-8 assay and FCM, respectively. The growth curves (Figure 2B) clearly showed the proliferation ability of $CD90^+$ cells and BEL-7404. Flow cytometry was used to analyze the change of expression of CD90 in $CD90^+$ LCSCs cultured with DMEM containing 10% FBS for 1 week. As shown in Figure 2C, the percentage of $CD90^+$ cells dramatically decreased with culture time. After 1 week, the percentage of $CD90^+$ cells had dropped to 3.2%, which was similar to the percentage in non-sorted BEL-7404 cells. The increase of OD value in the $CD90^+$ LCSCs group was due not to the fast proliferation of $CD90^+$ cells but to an increase in the number of $CD90^-$ cells. The expression of CD90 has been declining during 7 days of culture in the differentiation assay in Figure 2C. These results demonstrate that $CD90^+$ LCSCs, which are a small and rare subset of BEL-7404 cells, have a capacity for self-renewal and differentiation to produce descendent $CD90^-$ cells in culture.

Previous studies have shown that several tumors have elevated expression of CSC marker genes, and that this expression is associated with multi-drug resistance.[20,21] To determine the multi-drug resistance of $CD90^+$ LCSCs, the cells were treated with DOX, 5-FU, and OXA at different concentrations, and the IC50 values were calculated. Compared to $CD90^-$ BEL-7404 cells, $CD90^+$ LCSCs were more resistant to DOX, 5-FU, and OXA (Figure 2D). The IC50 value for the DOX-treated $CD90^+$ LCSCs was around sevenfold higher ($P<0.05$) than $CD90^-$ BEL-7404 cells (2.0 μg/mL). The IC50 value of 5-FU was 60.91±3.09 μg/mL for $CD90^-$ BEL-7404 cells and 290.19±9.07 μg/mL for $CD90^+$ LCSCs. The IC50 value of OXA was 10.87±4.09 μg/mL for $CD90^-$ BEL-7404 cells and 200.09±8.63 μg/mL for $CD90^+$ LCSCs. Taken together, these results demonstrate that $CD90^+$ LCSCs have obvious multi-drug resistance.

To demonstrate the stem-like traits of $CD90^+$ LCSCs in vivo, MACS-sorted hepatic carcinoma cells including $CD90^+$ and $CD90^-$ cells were subcutaneously injected into the right legs of nude mice. LCSCs formed tumors in the legs of all mice after 2 weeks, while the same number $CD90^-$ BEL-7404 cells did not generate tumors over the same observation time. Only two of the mice which injected with $CD90^-$ BEL-7404 cells had formed tumors after 16 weeks. H&E staining of the $CD90^+$ LCSCs and BEL-7404 cell tumors showed similar histology features (Figure 2E). Immunohistochemical staining results suggested that the majority of $CD90^+$ LCSCs differentiated into $CD90^-$ cells in tumor xenografts. In addition, the number of $CD90^+$ cells was consistent between the $CD90^+$ LCSCs transplantation group and the parent BEL-7404 established tumor. The expression rates of the $CD90^+$ LCSCs transplantation group and the parent BEL-7404 established tumor group are 7.77%±2.78% and 8.67%±3.27%, respectively (Figure 2E). This observation is consistent with past reports showing that the CSC population is often found to represent very few numbers in CSC-induced xenograft tumors.[22] It means that the $CD90^+$ cells showed the self-renewal and differentiation potential to produce descendent $CD90^-$ cells in vivo. Taken together, compared to $CD90^-$ BEL-7404, $CD90^+$ LCSCs were capable of self-renewal and have strong stem-like features.

Effects of magnetic hyperthermia on apoptosis rate and HSP90 expression

$CD90^+$ LCSCs were incubated with the CD90@TMs for 24 hours before being placed on an ACMF (f=200 kHz; I=20 A) to achieve a thermal dose (43°C) within 1 hour. To investigate the heat tolerance in $CD90^+$ LCSCs after magnetic hyperthermia, the expression level of HSP90 was examined after 10 minutes, 4 hours, 8 hours, 12 hours, 24 hours of culture time after heat treatment. HSP90 in $CD90^+$ LCSCs was up-regulated by heat treatment under the thermal dose of 43°C compared to the control group which was cultured with the medium (Figure 3A and B). The expression of HSP90 dramatically increased after magnetic hyperthermia plus 8-hour culture and continued to increase before peaking at 12 hours. The expression of caspase-3 was detected by Western blotting at 24 hours after heat treatment to determine if the inhibition of HSP90 could sensitize $CD90^+$ LCSCs to magnetic hyperthermia. As shown in Figure 3C and D, inhibition of HSP90 by 17-AAG could significantly sensitize $CD90^+$ LCSCs to magnetic hyperthermia, and increased expression of caspase-3. To further determine the effect of HSP90 inhibition upon hyperthermia and apoptosis, $CD90^+$ LCSCs were cultured with 17-AAG (5 μg/mL) before heat treatment. Cells showed an obviously higher apoptosis rate after

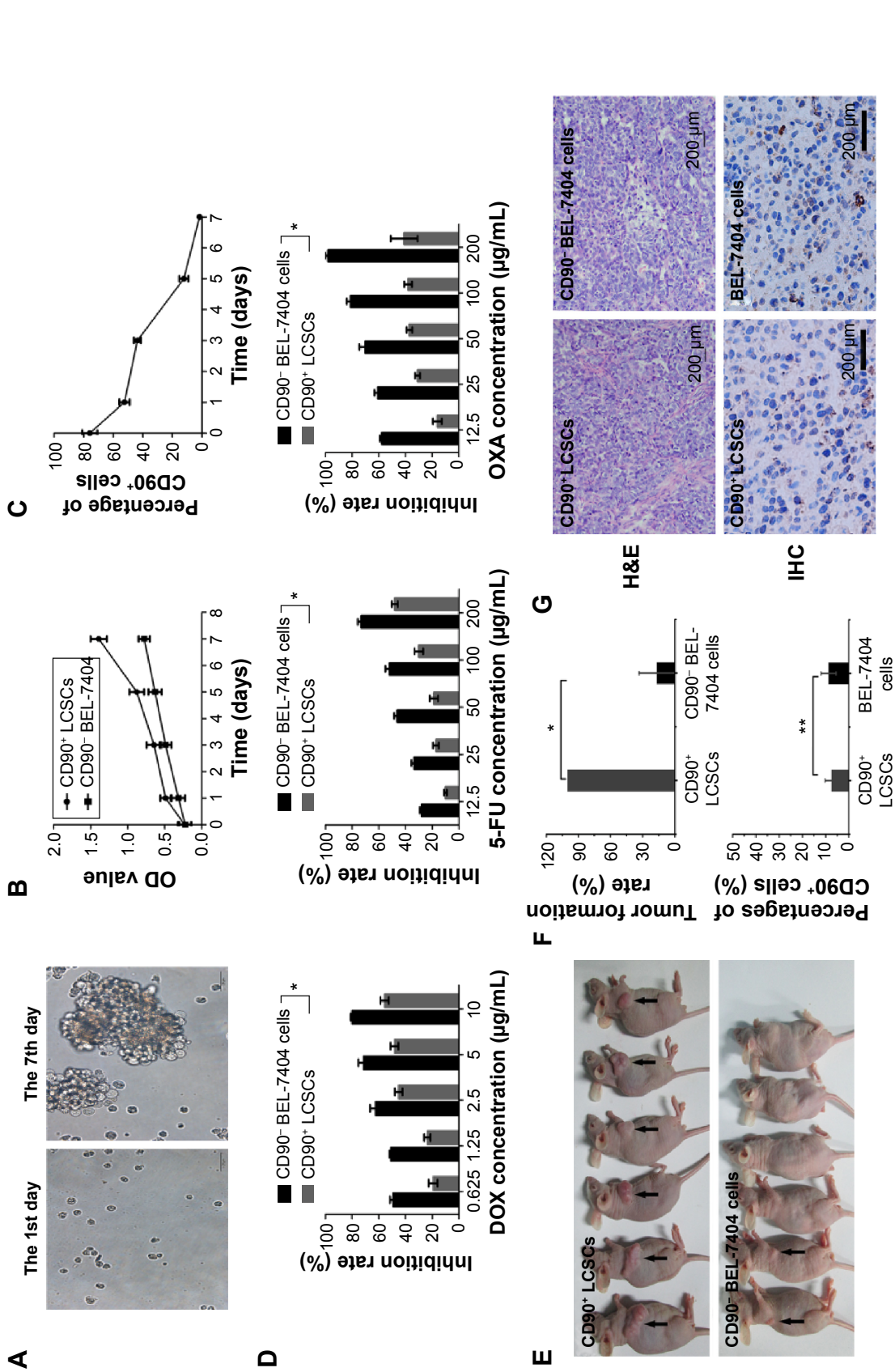

Figure 2 Identification of stem cell characteristic.

Notes: Identification of stem cell characteristics: (**A**) spheroid colony formation assay of CD90$^-$ LCSCs in 7 days; (**B**) proliferation assay of CD90$^+$ LCSCs and CD90$^-$ BEL-7404 cells in 7 days; (**C**) differentiation capacity of CD90$^+$ LCSCs in vitro in 7 days; (**D**) multi-drug resistance of CD90$^+$ LCSCs; (**E**) tumor formation assay through subcutaneous injection of MACS-sorted hepatic carcinoma cells including CD90$^+$ and CD90$^-$ cells into the right leg of nude mice and H&E staining of the xenografted tumor. The black arrows indicate the area of transplantation. *$P<0.05$. (**F**) Tumor formation rate of CD90$^-$ and CD90$^-$ cells, and the percentage of CD90$^+$ cells in the tumors established by isolated CD90$^+$ cells and parent BEL-7404 cells, respectively. (**G**) H&E staining for xenograft tumor established by CD90$^+$ cells and CD90$^-$ cells, respectively; and IHC staining for xenograft tumor established by CD90$^+$ cells and parent BEL-7404, respectively. Scale bar =200 μm. *$P<0.05$; **$P>0.05$.

Abbreviations: LCSCs, liver cancer stem-like cells; DOX, doxorubicin; 5-FU, 5-fluorouracil; OXA, oxaliplatin; H&E, hematoxylin-eosin; MACS, magnetic-activated cell sorting; IHC, immunohistochemical; OD, optical density.

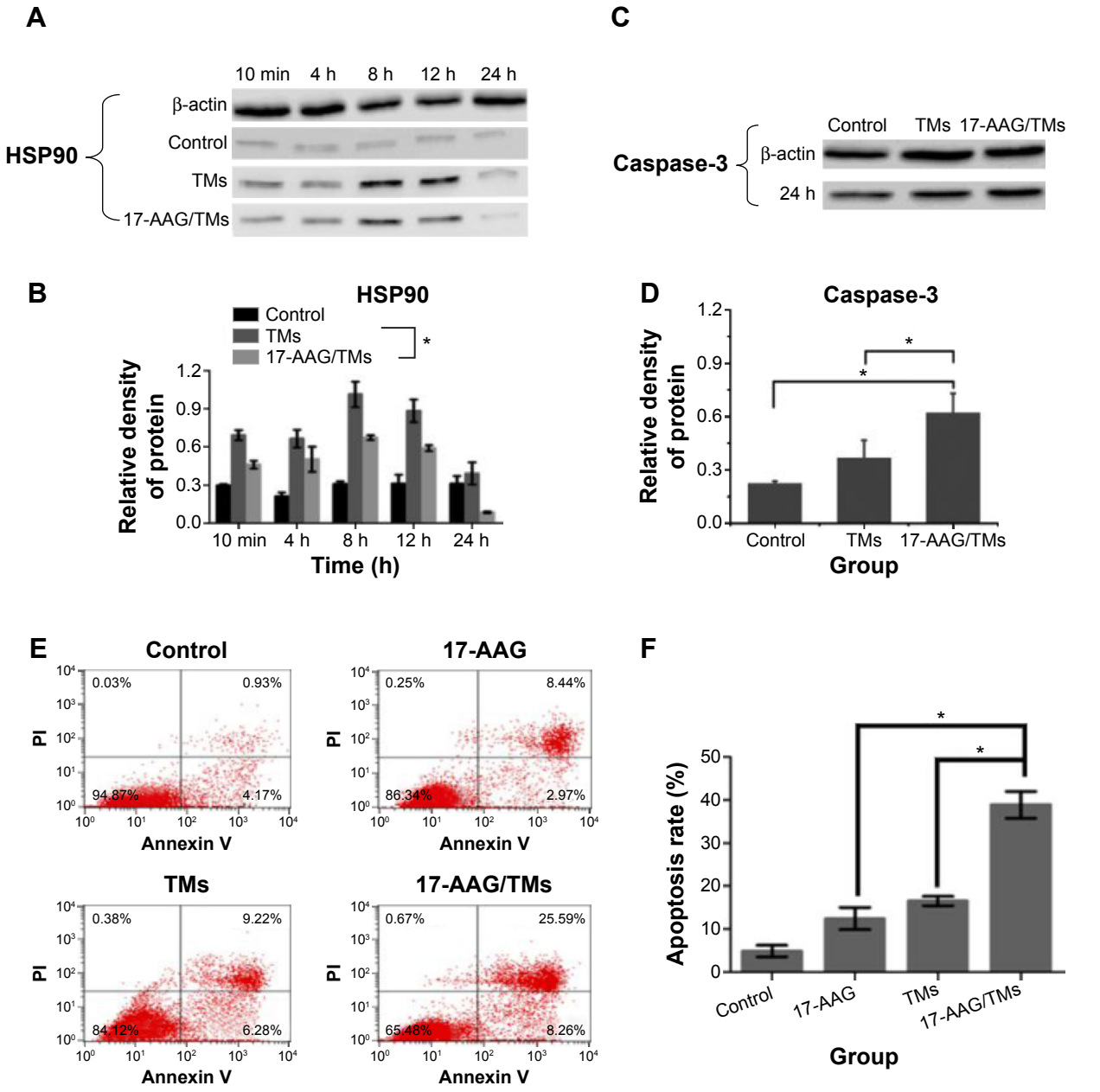

Figure 3 Inhibition of HSP90-sensitized CD90$^+$ LCSCs to magnetic hyperthermia-introduced apoptosis.

Notes: In the control group, cells were incubated with culture medium. In the TMs group, cells were incubated with TMs and exposed to ACMF. In the 17-AAG/TMs group, cells were incubated with 17-AAG and TMs and exposed to ACMF. (**A**) Expression of HSP90 observed by Western blot in CD90$^+$ LCSCs after 10 min, 4 h, 8 h, 12 h, 24 h of culture time following heat treatment. (**B**) Relative density of HSP90 after 10 min, 4 h, 8 h, 12 h, 24 h of culture time following treatment. (**C**) Expression level of caspase-3 in CD90$^+$ LCSCs after 24 h of culture time following heat treatment observed by Western blot. (**D**) Relative density of caspase-3 after 12 h after heat treatment. (**E** and **F**) Effects of inhibition of HSP90 on apoptosis rate in CD90$^+$ LCSCs. *$P<0.05$.

Abbreviations: HSP90, heat-shock protein; LCSCs, liver cancer stem-like cells; TMs, thermosensitive magnetoliposomes; 17-AAG, 17-allylamino-17-demethoxgeldanamycin; ACMF, alternating current magnetic field; 17-AAG/TMs, thermosensitive magnetoliposomes-encapsulated 17-AAG; 17-AAG/TSLs, 17-AAG-loaded thermosensitive liposomes; d, days; h, hours; min, minutes; PI, propidium iodide.

treated with 17-AAG combined with magnetic hyperthermia after 12 hours of culture as compared to the hyperthermia only group at the same thermal dose (Figure 3E and F). Meanwhile, the expression of HSP90 in the group pre-cultured with 17-AAG was significantly decreased after heat treatment compared to the hyperthermia only group. Therefore, these studies demonstrated that CD90$^+$ LCSCs are thermoresistant, which is a trait that occurs in the early stages of thermotherapy. The increased expression of HSP90 seemed to inhibit apoptosis of CD90$^+$ LCSCs. The inhibition of HSP90 by 17-AAG-sensitized CD90$^+$ LCSCs to magnetic hyperthermia-induced apoptosis.

All organisms produce a series of proteins called HSPs under stressful states such as high temperature and biological

stress. Heat treatment can activate apoptosis in tumor cells. Meanwhile, the intrinsic sensitivity of tumor cells to heat treatment is the essential factor that dictates therapy success. HSP90, which is overexpressed in high-temperature conditions, directly affects the effect of hyperthermia therapy. Studies have confirmed that heat-induced HSP90 expression protects cells by preventing protein degradation, and thus leads to thermoresistance.[23,24] Although cancer stem cells show poor response to radiotherapy and chemotherapy, thermotherapy can effectively eliminate cancer stem cell and inhibit their stem cell-like properties.[13] In this study, inhibiting the thermoresistance of $CD90^+$ LCSCs markedly enhanced the thermal-induced apoptosis. Therefore, inhibiting HSP90 is an effective method to kill cancer cells by enhancing the effects of thermotherapy.

The inhibition of HSP90 sensitizes LCSCs to magnetic hyperthermia and enhances anti-tumor effect on HCC-burdened nude mice

In a previous study, we demonstrated that 17-AAG inhibited the thermoresistance of $CD90^+$ LCSCs and markedly enhanced thermal-induced apoptosis. In addition, 17-AAG can induce tumor cell death by inhibiting the signal transduction pathway for cell proliferation and survival. Therefore, CD90@17-AAG/TMs were utilized to kill $CD90^+$ LCSCs by combining targeted therapy, thermotherapy, and chemotherapy. In an initial attempt to determine the effect of CD90@17-AAG/TMs to $CD90^+$ LCSCs in vitro, the apoptosis rate of cells in each group was observed. Figure 4A shows microscopic images of $CD90^+$ LCSCs in control and experimental groups. Cells in the control group adhered and grew well. In all groups except for the TSL, TM, and ACMF groups, the cells were noticeably deformed and smaller compared to control. The most prominent changes occurred in the CD90@17-AAG/TMs + ACMF-treated group. The apoptosis rates are shown in Figure 4B. As shown in Figure 4C, the apoptosis rate of cells treated with 17-AAG/TMs + ACMF was approximately three times higher (47.49%±1.21%) than the TMs + ACMF group (12.5%±0.97%) and the 17-AAG/TSLs group (24.26%±1.8%), which suggests that this formulation could kill $CD90^+$ LCSCs and effectively enhance the thermal-induced apoptosis. In addition, a significant increase in cell apoptosis was observed after hyperthermia and treatment with 17-AAG and Fe_3O_4 incorporated CD90-conjugated TMs. The apoptosis rate in the CD90@17-AAG/TMs + ACMF group was significantly higher than in the 17-AAG/TMs + ACMF and CD90@TMs + ACMF group. It means that inhibition of HSP90 by 17-AAG could sensitize $CD90^+$ LCSCs to magnetic hyperthermia. In addition, the CD90@TMs + ACMF group had a higher apoptosis rate than the TMs + ACMF group. This may be due to the fact that the targeted nanoparticles more easily entered $CD90^+$ liver cancer cells. A higher level of magnetic particle uptake by cells could contribute to an increase in intracellular hyperthermia, and ultimately a decrease in cell viability. The control, TM alone, TSLs, and ACMF groups showed identical apoptosis rates, which means that the TMs we prepared showed no cytotoxicity. These observations indicate that the inhibition of thermoresistance is critical for effective apoptotic hyperthermia, and that the combination of targeted therapy, thermotherapy, and chemotherapy could more effectively eliminate $CD90^+$ LCSCs.

Subsequently, the ability of CD90@17-AAG/TMs to work in vivo was assessed in nude mice. The effect was assessed by determining tumor volume over a treatment period of 7 days, and by examining H&E staining at the end of the treatment period. Since TM treatment alone showed no effects on $CD90^+$ LCSCs in vitro, the mice were divided into nine groups: control group, TMs + ACMF group, 17-AAG/TSLs group, 17-AAG/TMs + ACMF group, CD90@TMs + ACMF group, TSLs group (tumors injected with TSLs), 17-AAG group, ACMF group, and CD90@17-AAG/TMs + ACMF group. The CD90@17-AAG/TMs + ACMF group had the most significant reduction in tumor size compared to control ($P<0.05$). The tumor volume inhibit rate of the TM + ACMF group and the 17-AAG/TSLs group was higher than the control group (Figure 5A). The inhibition rate of tumor volume increased to 83.44%±5.78% in the CD90@17-AAG/TMs + ACMF group and more than 1.5-fold in the 17-AAG/TMs + ACMF group. The inhibition rates of tumor volume of the 17-AAG/TMs + ACMF and CD90@TMs + ACMF groups are 35.23%±4.67% and 61.44%±3.45%, respectively. It means that inhibiting the expression of HSP90 can slow the growth of tumor by increasing the sensitivity of $CD90^+$ LCSCs to magnetic hyperthermia. In contrast, the tumor volume of the TSLs group and ACMF group nearly showed no inhibition effect on the growth of the tumor. On day 7, all mice were sacrificed. H&E staining and a TUNEL assay were performed. As shown in Figure 5B, visible Fe_3O_4 sediment (red arrows) was found in the tumor tissues (black arrows) taken from thermotherapy groups and these sediments were surrounded by necrotic tumor cells (green arrows). The most severe damage occurred in the CD90@17-AAG/TMs + ACMF group, which may explain why the highest decrease

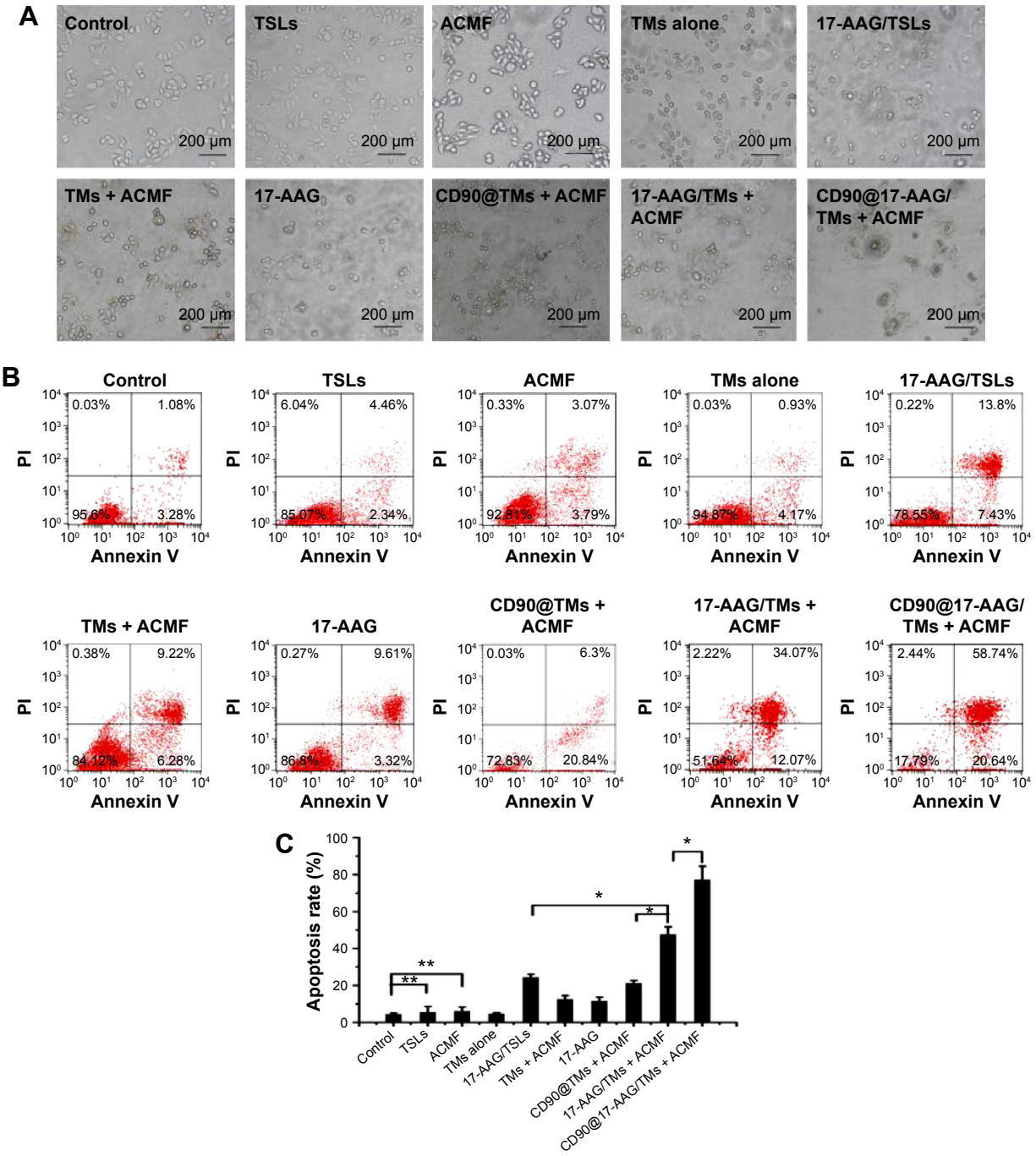

Figure 4 Inhibition of CD90+ LCSCs in vitro using CD90@17-AAG/TMs.

Notes: (**A**) Optical microscope images of CD90+ LCSCs after treatment with different therapeutic methods. Scale bars =200 μm. (**B**) Flow cytometric analysis of apoptosis in different experimental groups. (**C**) Apoptosis rates in different experimental groups. *$P<0.05$, **$P>0.05$.

Abbreviations: HSP90, heat-shock protein; LCSCs, liver cancer stem-like cells; TMs, thermosensitive magnetoliposomes; TSLs, thermosensitive liposomes; 17-AAG, 17-allylamino-17-demethoxygeldanamycin; 17-AAG/TMs, thermosensitive magnetoliposomes-encapsulated 17-AAG; 17-AAG/TSLs, 17-AAG-loaded thermosensitive liposomes; ACMF, alternating current magnetic field; CD90@17-AAG/TMs, CD90-targeted thermosensitive magnetoliposomes-encapsulated 17-AAG; CD90@TMs, TMs coupled with anti-CD90.

in tumor volume also occurred in this group. To identify the cell apoptosis rate in vivo, TUNEL staining (Figure 5C) was performed. The largest number of TUNEL-positive cells was found in the tumor tissues of the CD90@17-AAG/TMs + ACMF group, shown in Figure 5D. A significant difference was detected between the CD90@17-AAG/TMs + ACMF group and the other groups ($P<0.05$). However, it is a very small population of CD90+ cells in liver cancer. To address CD90@17-AAG/TMs are also more effective than 17-AAG/TMs in parent BEL-7404 established tumor, the mice were divided into three groups: control group, 17-AAG/TMs + ACMF group, and CD90@17-AAG/TMs + ACMF group. Tumor volume inhibition rate of the CD90@17-AAG/TMs group was significantly higher than those in the 17-AAG/

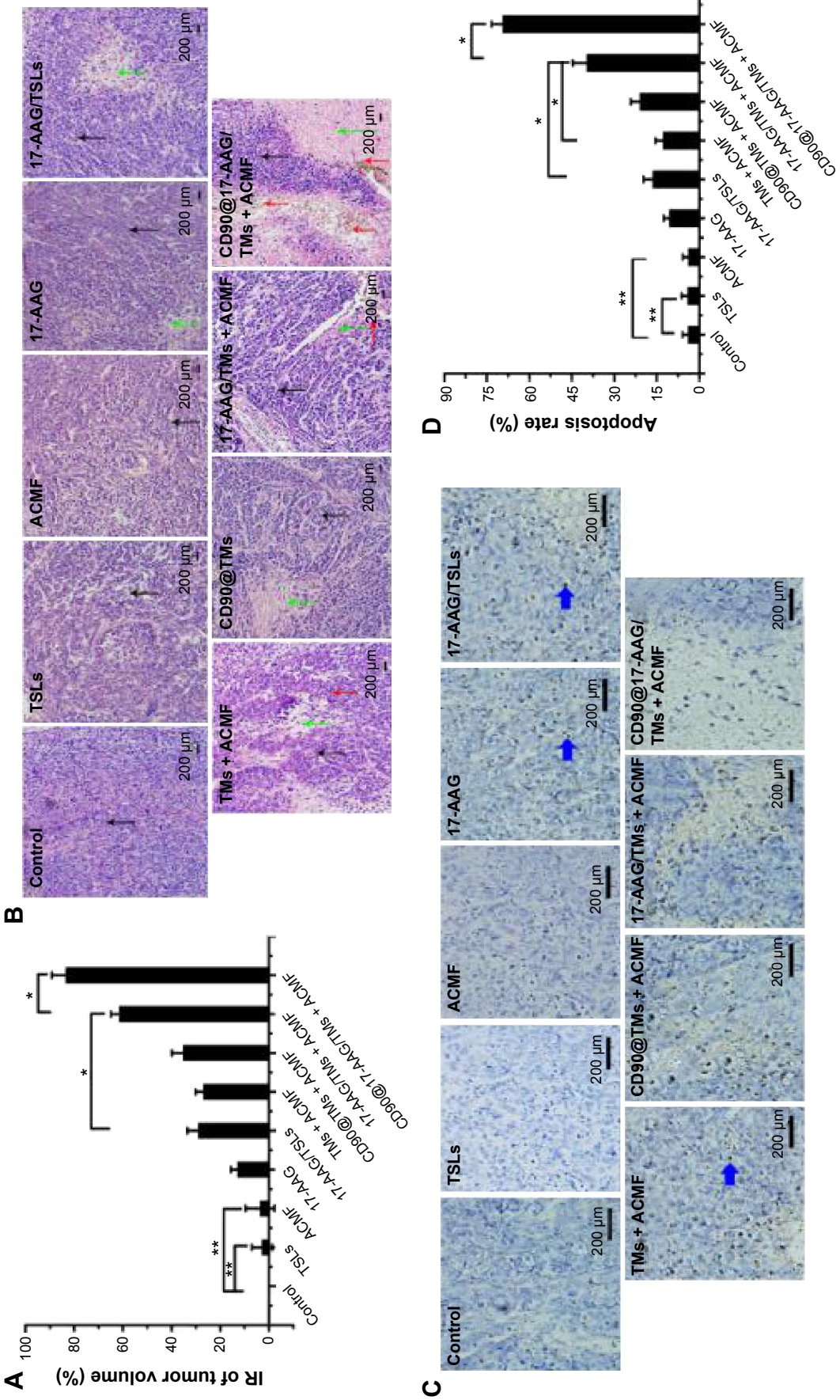

Figure 5 Inhibition of the growth of tumor in $CD90^+$ LCSC-bearing mice by CD90@17-AAG/TMs.

Notes: (**A**) Inhibition rate of tumor volume in different experimental groups (mean ± SD, n=6). (**B**) Tumor tissues of $CD90^+$ LCSC-bearing mice stained by H&E (the black arrows indicate the tumor tissues; the green arrows indicate the necrosis and collapse of tumor cells; the red arrows indicate the magnetic nanomaterial). Scale bars =200 μm. (**C**) Tumor tissues of $CD90^+$ LCSC-bearing mice stained by the TUNEL assay (the blue arrows indicate the typical apoptosis characteristics). Scale bars =200 μm. (**D**) Apoptotic cells in tumor tissues of $CD90^+$ LCSC-bearing mice (mean ± SD, n=6). To assess the fraction of apoptotic cells the count of TUNEL-positive cells was calculated from five sections. $^*P<0.05$, $^{**}P>0.05$.

Abbreviations: IR, inhibition rate; TSLs, thermosensitive liposomes; HSP90, heat-shock protein; LCSCs, liver cancer stem-like cells; TMs, thermosensitive magnetoliposomes; 17-AAG, 17-allylamino-17-demethoxygeldanamycin; 17-AAG/TMs, thermosensitive magnetoliposomes-encapsulated 17-AAG; 17-AAG/TSLs, 17-AAG-loaded thermosensitive liposomes; ACMF, alternating current magnetic field; H&E, hematoxylin-eosin; CD90@17-AAG/TMs, CD90-targeted thermosensitive magnetoliposomes-encapsulated 17-AAG; CD90@TMs, TMs coupled with anti-CD90; TUNEL, transferase-mediated deoxyuridine triphosphate-biotin nick end labeling.

TMs group (Figure 6A). The results of the H&E staining and TUNEL assay were shown in Figure 6B and C. The apoptotic cells in CD90@17-AAG/TMs + ACMF group were higher than the cells in 17-AAG/TMs + ACMF group (Figure 6D). CD90@17-AAG/TMs was also more effective than 17-AAG/TMs on the treatment of parent BEL-7404 established tumor. In conclusion, CD90@17-AAG/TMs-sensitized CD90$^+$ LCSCs to magnetic hyperthermia and enhanced the anti-tumor effect on HCC-burdened nude mice.

Since CSCs are related to relapse, metastasis, and tumor treatment resistance, therapeutic approaches targeting CSCs are expected to improve the treatment of cancer.[25] At present, routine clinical therapies target proliferating cancer cells rather than dormant or slow-growing CSCs, which often result in relapse.[26] Although treatments may successfully shrink a tumor, the tumor CSCs remain. Therefore, developing effective therapies focused on targeting cancer stem cells as a supplement to routine treatment are essential to lowering relapse occurrence and reducing mortality rates.

Magnetic hyperthermia has many advantages for tumor therapy. When combined with radiotherapy or chemotherapy, it not only reduces the dosage, and ultimately side effects due to the lowered dose, but also kills the cancer cells in the whole cell cycle, which enhances the therapeutic effect.[27] More importantly, magnetic hyperthermia has been reported to effectively eliminate CSCs' tumorigenic ability.[13] In our previous study, we demonstrated that magnetic hyperthermia could not only kill CD90$^+$ LCSCs in vitro, but also inhibit tumor growth in nude mice bearing CD90$^+$ LCSCs. Therefore, magnetic hyperthermia for the destruction of CSCs is a promising therapeutic method for tumor therapy. There is still no clear consensus about the mechanism of thermotherapy. Tumor thermotherapy is a typical stress stimulation that triggers cell death and protective mechanisms.[28] Thermoresistance is also an important factor that affects the effectiveness of sub-high-temperature thermotherapy.[29] HSP90 is one of the most active chaperone proteins in cells. Since the expression of HSP90

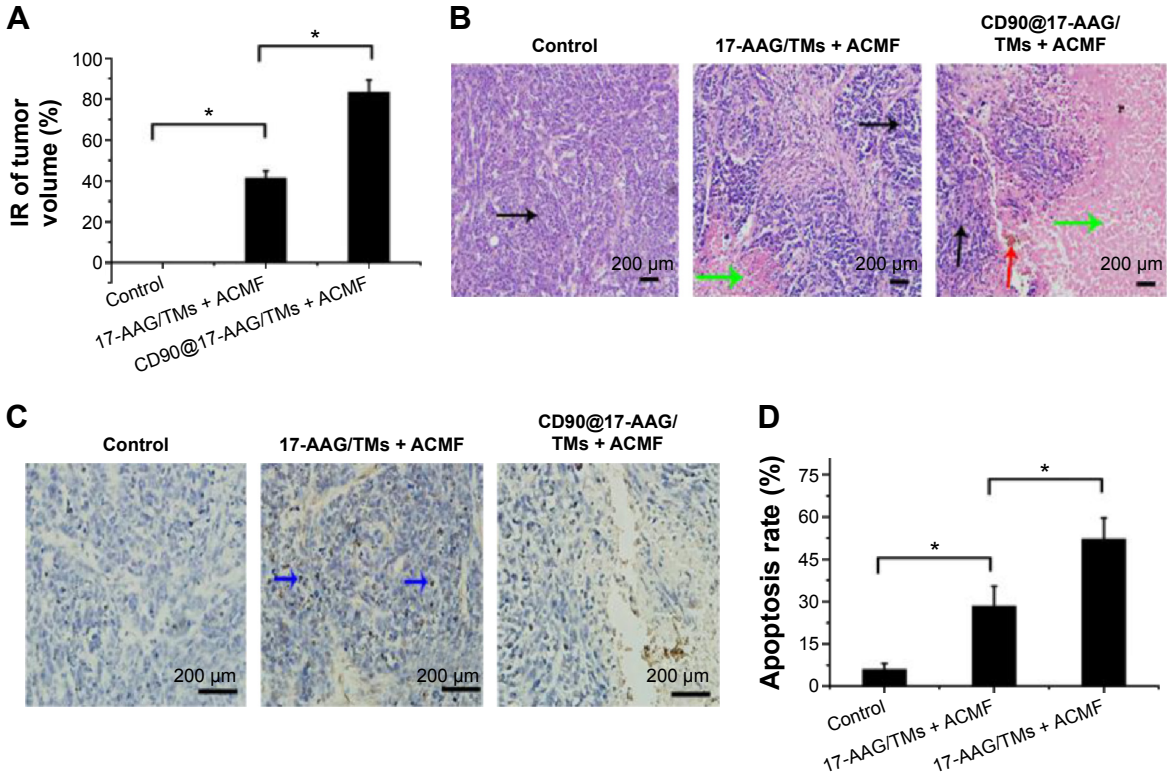

Figure 6 Inhibition of the growth of tumor in BEL-7404 cell-bearing mice by CD90@17-AAG/TMs.

Notes: (**A**) Inhibition rate of tumor volume in different experimental groups (mean ± SD, n=6). (**B**) Tumor tissues of BEL-7404 cells-bearing mice stained by H&E (the black arrows indicate the tumor tissues; the green arrows indicate the necrosis and collapse of tumor cells; the red arrows indicate the magnetic nanomaterial). Scale bars =200 μm. (**C**) Tumor tissues of BEL-7404 cells-bearing mice stained by TUNEL assay (the blue arrows indicate the typical apoptosis characteristics). Scale bars =200 μm. (**D**) Apoptotic cells in tumor tissues of BEL-7404 cell-bearing mice (mean ± SD, n=6). To assess the fraction of apoptotic cells, the count of TUNEL-positive cells was calculated from five sections. *$P<0.05$.

Abbreviations: IR, inhibition rate; HSP90, heat-shock protein; LCSCs, liver cancer stem cells; TMs, thermosensitive magnetoliposomes; 17-AAG, 17-allylamino-17-demethoxgeldanamycin; 17-AAG/TMs, thermosensitive magnetoliposomes-encapsulated 17-AAG; ACMF, alternating current magnetic field; H&E, hematoxylin-eosin; CD90@17-AAG/TMs, CD90-targeted thermosensitive magnetoliposomes-encapsulated 17-AAG; CD90@TMs, TMs coupled with anti-CD90; TUNEL, transferase-mediated deoxyuridine triphosphate-biotin nick end labeling.

is mediated by thermoresistance, and many of HSP90's effector proteins are the protein kinases or transcription factors that regulate cell survival and apoptosis, the inhibition of HSP90 is predicted to make tumors more sensitive to hyperthermia therapy.[30] In addition, compared to normal tissues, the expression of HSP90 is prominently enhanced in tumor tissues, which suggests that HSP90 is one of the most promising targets to improve the efficacy of cancer treatments. The effects of HSP90 inhibition on tumor cells during hyperthermia therapy could effectively result in apoptosis at low temperatures without resulting in thermoresistance.[7,31] However, thermoresistance in CSCs has not been reported. In this study, we first researched the expression of HSP90 in $CD90^+$ LCSCs subjected to magnetic hyperthermia, and we then demonstrated that inhibiting HSP90 could significantly enhance the sensitivity of $CD90^+$ LCSCs to magnetic hyperthermia both in vitro and in vivo.

Studies have reported that 17-AAG, an HSP90 molecular chaperone complex retardant, does not only enhance the radiotherapy and thermotherapy sensitivity of tumor cell, but also reduces tolerance without affecting normal cells.[32,33] In addition, as a unique tumor treatment, 17-AAG can effectively inhibit many cell signal transduction pathways that maintain the proliferation and survival of tumor cells.[34] Hence, we propose a brand-new combined therapy that targets cancer stem cells. In this therapy, physical targeting is combined with biological targeting using an anti-CD90 monoclonal antibody to ensure specificity. In addition, magnetic nano-particle-induced heating is combined with biological therapy using 17-AAG to guarantee the effectiveness of the treatment.

Conclusion

In this study, CSCs from liver cancer cells were successfully isolated and characterized. A targeted magnetic nanocarrier, coupled with an anti-CD90 monoclonal antibody, with 17-AAG inside, can effectively inhibit thermoresistance and enhance the thermotherapy sensitivity of CSCs in vitro and in vivo. In addition, the composite nanomaterial combined with magnetic induction heating prominently inhibited the tumor growth in nude mice bearing $CD90^+$ liver stem cells.

Acknowledgments

This work was supported by the National Key Basic Research Program of China (973 Program) (Grant numbers 2013 CB933904 and 2011CB933500), National Natural Science Foundation of China (81271635, 81301270, and 81201131), National Natural Science Foundation of Jiangsu Province (BK2012335), the Fundamental Research Funds for the Central Universities and the Regular University Graduate Student Scientific Research Innovation Projects of Jiangsu Province (KYLX_0204), and the Scientific Research Foundation of the Graduate School of Southeast University and Southeast University Excellent Doctor Degree Thesis Training Fund (YBJJ1459).

Disclosure

The authors report no conflicts of interest in this work.

References

1. Liao SH, Liu CH, Bastakoti BP, et al. Functionalized magnetic iron oxide/alginate core–shell nanoparticles for targeting hyperthermia. *Int J Nanomed*. 2015;10:3315.
2. Oliveira TR, Stauffer PR, Lee CT, et al. Magnetic fluid hyperthermia for bladder cancer: a preclinical dosimetry study. *Int J Hyperthermia*. 2013;29(8):835–844.
3. Kossatz S, Grandke J, Couleaud P, et al. Efficient treatment of breast cancer xenografts with multifunctionalized iron oxide nanoparticles combining magnetic hyperthermia and anti-cancer drug delivery. *Breast Cancer Res*. 2015;17(1):66.
4. Moros M, Ambrosone A, Stepien G, et al. Deciphering intracellular events triggered by mild magnetic hyperthermia *in vitro* and *in vivo*. *Nanomedicine (Lond)*. 2015;10(14):2167–2183.
5. Calderwood SK. Hyperthermia, the tumor microenvironment and immunity. In: *Tumor Ablation*. Yona Keisari, editor. Dordrecht, the Netherlands: Springer; 2013:29–37.
6. Duncan RF. Inhibition of HSP90 function delays and impairs recovery from heat shock. *FEBS J*. 2005;272(20):5244–5256.
7. Yoo D, Jeong H, Noh SH, et al. Magnetically triggered dual functional nanoparticles for resistance – free apoptotic hyperthermia. *Angew Chem Int Ed*. 2013;52(49):13047–13051.
8. Kaluarachchi WD, Curley SA. Multimodality therapy: enhancement of melanoma cell death with combination of heat shock protein 90 inhibitor, 17-(allylamino)-17-demethoxygeldanamycin (17-AAG), and gold nanoparticles in a noninvasive radiofrequency field. *Proceedings of Nanotechnology 2010: Bio Sensors, Instruments, Medical, Environment and Energy-Technical Proceedings of the 2010 NSTI Nanotechnology Conference and Expo, NSTI-Nanotech 2010*. 2010;3:409–411.
9. Katragadda U, Fan W, Wang Y, et al. Combined delivery of paclitaxel and tanespimycin via micellar nanocarriers: pharmacokinetics, efficacy and metabolomic analysis. *PLoS One*. 2013;8(3):e58619.
10. Yang ZF, Ho DW, Ng MN, et al. Significance of $CD90^+$ cancer stem cells in human liver cancer. *Cancer Cell*. 2008;13(2):153–166.
11. Zhou J, Hu Z, Li Z, et al. The role of liver cancer stem cells in donor liver allocation for patients with hepatocellular carcinoma. *Postgrad Med*. 2013;125(6):24–30.
12. Bahnassy AA, Zekri AR N, El-Bastawisy A, et al. Circulating tumor and cancer stem cells in hepatitis C virus-associated liver disease. *World J Gastroenterol*. 2014;20(48):18240.
13. Sadhukha T, Niu L, Wiedmann TS, et al. Effective elimination of cancer stem cells by magnetic hyperthermia. *Mol Pharm*. 2013;10(4):1432–1441.
14. Li Y, Liu J, Zhong Y, et al. Biocompatibility of Fe_3O_4@Au composite magnetic nanoparticles *in vitro* and *in vivo*. *Int J Nanomed*. 2011;6:2805.
15. Wang L, Zhang J, An Y, et al. A study on the thermochemotherapy effect of nanosized As_2O_3/MZF thermosensitive magnetoliposomes on experimental hepatoma *in vitro* and *in vivo*. *Nanotechnology*. 2011;22(31):315102.

16. Boot EP, Koning GA, Storm G, et al. CD134 as target for specific drug delivery to auto-aggressive CD4+ T cells in adjuvant arthritis. *Arthritis Res Ther*. 2005;7(3):R604–R615.
17. Wu KS, Tang JT, Liu X, et al. Preparation of magnetoliposomes and its *in vivo* behavior on ICR mice. *Acta Pharm Sin*. 2004;39(4):288–291.
18. Yang R, An YL, Miao FQ, et al. Preparation of folic acid-conjugated, doxorubicin-loaded, magnetic bovine serum albumin nanospheres and their antitumor effects *in vitro* and *in vivo*. *Int J Nanomed*. 2014; 9:4231.
19. Xie J, Yan C, Zhang Y, et al. Shape evolution of "multibranched" Mn–Zn ferrite nanostructures with high performance: a transformation of nanocrystals into nanoclusters. *Chem Mater*. 2013;25(18):3702–3709.
20. Sarvi S, Mackinnon AC, Avlonitis N, et al. $CD133^+$ cancer stem-like cells in small cell lung cancer are highly tumorigenic and chemoresistant but sensitive to a novel neuropeptide antagonist. *Cancer Res*. 2014;74(5):1554–1565.
21. Ding J, Wu J. Epigenetic regulation of hepatic tumor-initiating cells. *Front Biosci (Landmark edition)*. 2014;20:946–963.
22. Ma S, Chan KW, Hu L, et al. Identification and characterization of tumorigenic liver cancer stem/progenitor cells. *Gastroenterology*. 2007;132(7):2542–2556.
23. Miyagawa T, Saito H, Minamiya Y, et al. Inhibition of HSP90 and 70 sensitizes melanoma cells to hyperthermia using ferromagnetic particles with a low Curie temperature. *Int J Clin Oncol*. 2014;19(4):722–730.
24. Kudryavtsev VA, Makarova YM, Kabakov AE. Thermosensitization of tumor cells with inhibitors of chaperone activity and expression. *Biochem (Moscow) Suppl Ser B: Biomed Chem*. 2012;6(1):61–67.
25. Osaki M, Okada F, Ochiya T. miRNA therapy targeting cancer stem cells: a new paradigm for cancer treatment and prevention of tumor recurrence. *Ther Deliv*. 2015;6(3):323–337.
26. Haraguchi N, Ishii H, Mimori K, et al. CD13 is a therapeutic target in human liver cancer stem cells. *J Clin Invest*. 2010;120(9):3326.
27. Bañobre-López M, Teijeiro A, Rivas J. Magnetic nanoparticle-based hyperthermia for cancer treatment. *Reports Pract Oncol Radiother*. 2013;18(6):397–400.
28. Milani V, Noessner E. Effects of thermal stress on tumor antigenicity and recognition by immune effector cells. *Cancer Immunol Immunother*. 2006;55(3):312–319.
29. Tabuchi Y, Kondo T. Targeting heat shock transcription factor 1 for novel hyperthermia therapy (Review). *Int J Mol Med*. 2013;32(1):3–8.
30. Chehab M, Caza T, Skotnicki K, et al. Targeting HSP90 in urothelial carcinoma. *Oncotarget*, 2015.
31. Duncan RF. Inhibition of HSP90 function delays and impairs recovery from heat shock. *FEBS J*. 2005;272(20):5244–5256.
32. Huang HC, Yang Y, Nanda A, et al. Synergistic administration of photothermal therapy and chemotherapy to cancer cells using polypeptide-based degradable plasmonic matrices. *Nanomedicine*. 2011;6(3):459–473.
33. Xia M, Huang R, Sakamuru S, et al. Identification of repurposed small molecule drugs for chordoma therapy. *Cancer Biol Ther*. 2013;14(7): 638–647.
34. Kalmar B, Lu CH, Greensmith L. The role of heat shock proteins in amyotrophic lateral sclerosis: the therapeutic potential of Arimoclomol. *Pharmacol Therap*. 2014;141(1):40–54.